

Numerical Investigations of CO₂ as Fire Suppressing Agent

VISWANATH R. KATTA

Innovative Scientific Solutions Inc.

2766 Indian Ripple Road, Dayton, OH 45440

FUMIAKI TAKAHASHI

National Center for Microgravity Research on Fluids and Combustion

NASA Glenn Research Center

21000 Brookpark Road, Cleveland, OH 44135

GREGORY T. LINTERIS

Fire Research Division, National Institute of Standards and Technology

Gaithersburg, MD 20899

ABSTRACT

Understanding suppression mechanisms of different fire-suppressing agents including CF₃Br (Halon 1301) and inert gases is useful for their efficient use and for developing new agents. Because of the similarities between unsteady jet diffusion flames formed over the cup burner and uncontrolled fires, it is believed that studies of fire-suppressing agents in the former system could provide valuable information on the behavior of such agents in actual fires. In the present study, suppression characteristics of CO₂ were investigated in two flame systems: 1) a periodically oscillating, methane-air jet diffusion flame formed over a cup burner, and 2) a steady-state planar flame formed between opposing jets of fuel and air. A detailed chemical-kinetics model having 31 species and 346 elementary-reaction steps was used. Calculations made for the cup burner yielded a flame-flicker frequency of about 10 Hz. The suppression mechanisms promoted by CO₂ were investigated by adding CO₂ to the airflow, while maintaining the total flow rate constant, for both the cup-burner and opposed-jet flames. In the cup-burner flame, the addition of CO₂ reduced the flame temperature to ~1620 K at suppression. Addition of CO₂ destabilized the flame base, which then moved downstream in search of a new stabilization location. For CO₂ volume fractions greater than 14.5 %, the flame base moved out of the computational area, as it could not find a stabilization point within this domain. The unsteady flickering motion of the flame and higher concentrations of CO₂ accelerated this quenching process through blowout. Even for very high concentrations of CO₂, the calculations did not yield simultaneous quenching of the entire cup-burner flame. On the other hand, the opposed-jet flame was extinguished through the global extinction of flame chemistry. The low-strain (30 s⁻¹) opposed-jet flame extinguished for CO₂ volume fractions > 16.4 %, while the moderately strained (90 s⁻¹) flame extinguished for volume fractions > 10.4 %. Both the opposed-jet flames extinguished nearly at the same flame temperature (~1580 K), indicating that the extinction limits in these flames are primarily controlled by chemical kinetics.

KEY WORDS: fire suppression, flame extinction, pool fires

INTRODUCTION

Effective fire-extinguishing agents are known to act through 1) chemical mechanisms in which free-radical concentrations are reduced via agent chemistry and 2) physical mechanisms in which temperature is decreased due to dilution and thermal effects. While reduction in the oxygen concentration causes dilution effects, nearly inert agents with higher specific heat also cause thermal effects (by reducing the total heat release per unit mass of the mixture). Trifluorobromomethane (CF_3Br , Halon 1301), which primarily acts through chemical mechanisms, is a widely used [1] fire-suppressing agent and numerous studies have been conducted for understanding its inhibitory mechanism [2-4]. However, it is also extremely effective for depleting stratospheric ozone. Consequently, with the current ban on the production of CF_3Br , replacements that are predominantly fluorinated hydrocarbons are being considered [5]. Understanding the inhibition mechanisms of these replacements along with CF_3Br and inert agents is important for their efficient use and for developing new agents.

Studies conducted to gain an understanding of the inhibitory effects of halogenated hydrocarbons on flames have been performed in premixed [6,7] and diffusion systems [8,9]. Premixed flames are selected mainly because the overall reaction rate, heat release, and heat and mass transport can be described with a fundamental parameter—the laminar burning velocity; on the other hand, most common fires are of the diffusion type and often become dynamic in nature with large vortical structures entraining additional surrounding air.

The predominant experimental techniques for studying fire-suppression in diffusion flames are the cup-burner and opposed-jet configurations. In both experiments, agents are quasi-statically added to either the fuel or air stream. The non-premixed reactant streams in the cup burner flow parallel to each other, and the flame is stabilized in the shear layer formed between the two co-flowing streams. The resulting flame structure is axisymmetric and has features that are similar to fires. Studies on cup-burner flames are also important since the amount of agent required for extinguishing these flames is believed to scale to the requirements in fires. The opposed-jet configuration offers very simple flames that can be modeled using one-dimensional analysis and, hence, is often used for the development of chemical kinetics models for different agents. From a fire safety point of view, however, the most hazardous situation is a low-strain-rate diffusion flame such as the one established over a cup burner where flames are more stable and larger concentrations of agent are required to achieve extinction.

Under normal gravitational conditions, a laminar jet diffusion flame formed over a cup burner with a negligibly small fuel flow rate and a low-speed annular air flow develops large-scale, low-frequency (1-40 Hz), organized buoyancy-induced vortices on the air side of the flame—very similar to those seen in pool fires. Because of the similarities between the cup-burner diffusion flames and uncontrolled fires, the former may also be investigated to understand the effects of gravity on vortical structures, flame-vortex interactions, and entrainment characteristics of the latter. It is also believed that these unsteady effects could alter the agent requirements in extinguishing the fires that are established from the investigations of steady-state flames. The main objective of the present study is to investigate numerically the dynamic flames associated with the cup burner and identify the differences in agent requirements established using opposed-jet and cup-burner flames.

Several numerical investigations of dynamic jet flames were performed in the past using the conserved-scalar, global-chemistry, and detailed chemistry models, and have revealed important aspects of combustion such as the effect of heat-release rate [10,11], the role of buoyancy [12-14], enhancement of soot formation [15], and Lewis-number effects [16,17]. However, the authors are not aware of any comprehensive computation performed for the prediction of the effects of fire-suppressing agents on jet diffusion flames--mainly, because of the large chemical kinetics required for describing the inhibition action of the agents in hydrocarbon flames.

This paper describes a two-dimensional numerical method, with detailed kinetics, developed for the simulation of dynamic cup-burner diffusion flames extinguished by a fire suppressant. For a comparison purpose, steady state flames established between opposed-jet flows were also simulated using the same two-dimensional code.

NUMERICAL MODEL

A time-dependent, axisymmetric mathematical model known as UNICORN (Unsteady Ignition and Combustion using ReactionNs) [18] is used for the simulation of unsteady jet diffusion flames associated with the cup burner. It solves for axial and radial (z and r) momentum equations, continuity, and enthalpy- and species-conservation equations on a staggered-grid system. The body-force term due to the gravitational field is included in the axial-momentum equation to simulate upward-oriented flames. A clustered mesh system is employed to trace the gradients in flow variables near the flame surface. A detailed chemical-kinetics model GRI-V1.2 (developed by the Gas Research Institute) is incorporated in UNICORN for the investigation of CO_2 effects on methane combustion [19]. This mechanism for methane flames is comprehensive, with 31 species and 346 elementary reactions. Thermophysical properties such as enthalpy, viscosity, thermal conductivity, and binary molecular diffusion of all the species are calculated from the polynomial curve fits developed for the temperature range 300 - 5000 K. Mixture viscosity and thermal conductivity are then estimated using the Wilke and Kee expressions, respectively. Binary-type diffusion is assumed with the diffusion velocity of a species calculated using Fick's law and the effective-diffusion coefficient of that species in the mixture. A simple radiation model based on optically thin-media assumption was incorporated into the energy equation. Only radiation from CH_4 , CO , CO_2 , and H_2O was considered in the present study [20].

The finite-difference forms of the momentum equations are obtained using an implicit QUICKEST scheme [13], and those of the species and energy equations are obtained using a hybrid scheme of upwind and central differencing. At every time-step, the pressure field is accurately calculated by solving all the pressure Poisson equations simultaneously and utilizing the LU (Lower and Upper diagonal) matrix-decomposition technique. The boundary conditions are treated in the same way as that reported in earlier papers [21].

Unsteady axisymmetric calculations for the cup-burner flames are made on a physical domain of 200 x 47.5 mm utilizing a 251 x 101 non-uniform grid system that yielded 0.2-mm grid spacing in both the z and r directions in the flame zone. The computational domain is bounded by the axis of symmetry and a wall boundary in the radial direction and by the inflow and outflow boundaries in the axial direction. The outer boundary in z direction is located sufficiently far from the burner exit (~ 7.5 fuel cup diameters) such

that propagation of boundary-induced disturbances into the region of interest is minimal. Flat velocity profiles are imposed at the fuel and air inflow boundaries, while an extrapolation procedure with weighted zero- and first-order terms is used to estimate the flow variables at the outflow boundary. For the accurate simulation of flow structure at the base of the flame, which is very important in the flame-extinction studies, the fuel cup wall was treated as a 1-mm long and 1-mm thick tube in the calculations. The temperature of this tube was set at 600 K, which is very close to that measured in the experiment.

Simulations were performed on a Pentium III-1-GHz-based Personal Computer with 1 GB of memory. Typical execution time was ~ 52 s/time-step. Stably oscillating flames were obtained in about 3000 time-steps (which corresponds to 300 ms real time).

EXPERIMENT

The cup burner, described previously [22-24], was used for the present experiments. It consists of a cylindrical glass cup (28-mm diameter) positioned inside a glass chimney (53.3-cm tall, 9.5-cm diameter). To provide uniform flow, 6-mm glass beads fill the base of the chimney, and 3-mm glass beads (with two 15.8 mesh/cm screens on top) fill the fuel cup. Gas flows were measured by mass flow controllers (Sierra 860¹), which were calibrated so that their uncertainty is 2 % of indicated flow. (All uncertainties are expressed as expanded uncertainties with a coverage factor of two.) To determine the extinction condition, the co-flowing air was held constant at (41.6 ± 0.8) L/min, and CO₂ was added to the flow (in increments of < 1 % near extinction) until lift-off was observed. The air velocity in the absence of CO₂ is (10.7 ± 0.21) cm/s, and the fuel jet velocity is (0.921 ± 0.018) cm/s. The test was repeated at least three times. The fuel gas is methane (Matheson UHP, 99.9 %), the agent is CO₂ (Airgas), and the air is house compressed air (filtered and dried) which is additionally cleaned by passing it through an 0.01 μ m filter, a carbon filter, and a desiccant bed to remove small aerosols, organic vapors, and water vapor.

RESULTS AND DISCUSSION

The flow of non-premixed reactants in a direction parallel to each other in a cup burner results in an axisymmetric, two-dimensional flame. Typically, very low velocities are used for the reactant flows such that the flame generated is quite stable and its structure is similar to that of the uncontrolled fires. The fuel and air velocities of 0.921 and 10.7 cm/s, respectively, used in the present investigation represent a weakly strained flame. Several calculations were made for this flame to investigate the extinction behavior with different concentrations of CO₂ in the oxidizer stream.

The computed instantaneous flowfield in the base region of the pure CH₄/air flame is shown in color in Fig. 1. The iso-molar-concentration distributions of CH₄ and O₂ are shown in 1(a) on the left and right halves, respectively. The velocity field is also superimposed in this picture. Even though the instantaneous flame in the base region

¹ Certain commercial equipment, instruments, or materials are identified in this paper to adequately specify the procedure. Such identification does not imply recommendation or endorsement by NIST nor does it imply that the materials or equipment are necessarily the best available for the intended use.

resembles a steady-state one, the flame, in fact, is oscillating significantly at a low frequency. Because of the gravity term in the axial-momentum equation and the low-speed annular-air flow (10.7 m/s), solution of the governing equations resulted in a dynamic flame, with large toroidal vortices forming naturally outside the flame surface. As these vortices convect downstream, they cause the flame to squeeze at certain locations and bulge at others. It is important to note that no artificial perturbation either in the calculations or in the experiment is required for the development of these outer vortices. In the presence of gravitational force, acceleration of hot gases along the flame surface generated the vortical structures as part of the solution. Even though, these vortices (or instabilities) start to form well upstream in the flame near the base region, they develop into recognizable vortical structures only in the farther downstream locations ($z > 50$ mm). However, due to the formation and convection of the vortices, the flame surface oscillates radially at every location with varying intensity. The frequency corresponding to the passage of these vortices (also known as the flame-flickering frequency) is ~ 11 Hz.

Because of the very low fuel flow rate, the flame is squeezed inward [Fig. 1] and the velocity at the flame base no longer remains parallel to the flame surface. As a result, the flame at the base is subjected to moderate strain induced by the entraining air. The temperature and CO₂ concentrations at the same instant are shown in Fig. 1(b) in the left and right halves, respectively. Except in the base region ($0.1 < z < 4$ mm), the peak temperature of the flame is constant everywhere at 1880 K. The flame height at the instant shown in Fig. 1 is ~ 55 mm. The concentrations of important radicals CH₃ and OH are shown in Fig. 1(c). These radicals are generated in significant quantities in the base region compared to those generated in the downstream locations, making the flame structure at the base quite different.

Evolutions of the flame at two different heights above the burner are shown in Fig. 2 by plotting the radial distribution of temperature at different times. While the image in Fig. 1 represents the flame structure for most of the flame domain at $t = 100$ ms, that in Fig. 2 represents the temperature at two locations for approximately one cycle ($0 \text{ ms} < t < 100 \text{ ms}$). At $z = 30$ mm, the flame is oscillating radially, along with a weak fluctuation of fuel jet at the center. However, the vortices formed outside the flame surface have grown significantly by the time they reached a height of 80 mm and are pinching off a portion of fuel from the fuel jet. The detached fuel mass is burning separately as it convects downstream. These data are collected after discarding initial calculations made for the approximate 2 s transient period, after which the flame has reached a stably oscillating state. A comparison between evolutions at 30 and 80 mm reveals that the period of oscillation at the former location is ~ 105 ms ($f \sim 9.5$ Hz) while that at the latter location is ~ 93 ms ($f \sim 10.8$ Hz). This difference in oscillation frequency suggests that the evolution of one vortex is slightly different from that of the preceding one and that the evolutions plotted for the next 100 ms could be different from those shown in Fig. 2. Such difference was not observed in the previous studies on buoyant jet diffusion flames [25,26] and may be attributed to the confinement (chimney) used for the cup-burner flames. It is important to understand the differences in the oscillation frequencies at different heights since such variation could affect the flame extinguishment process, especially near the critical-concentration.

The structure of the flame at a height 10 mm above the burner is shown in Fig. 3, in which the temperature and species volume fraction distributions are plotted with respect

to radial distance. As expected, the oxygenated radicals (O, OH) peak on the airside of the flame and the methyl radicals (CH_3) peak on the fuel side. Fig. 3 also shows that significant amount of H_2 is produced ($\sim 3\%$) in this flame which is burned later at downstream locations.

To evaluate the extinction performance of CO_2 in this flame, a number of calculations were performed for increasing amounts of CO_2 in the air stream, with a constant co-flowing gas velocity at the cup rim. Replacing part of the air with an agent lowers oxygen mole fraction in the oxidizer stream, which affects the overall reaction rate in two ways: the concentrations of all reactants are lower, and the peak temperature is lower. To isolate these two effects, calculations can be performed by substituting the agent either for a part of the nitrogen (without altering the concentration of oxygen) or for a part of the air. Since for the case of CO_2 , the change in peak temperature is more important than the reduction in the reactant mole fractions, the calculations in the present study were performed only for the case of CO_2 replacing part of the air.

Since the annular air velocity is only ~ 0.11 m/s, the agent introduced into the calculations from the inflow boundary requires about 1.8 s (i.e., ~ 18000 time steps) to reach the exit boundary. To expedite the calculations, new initial data for the calculations with CO_2 were generated by replacing the corresponding amount of air with the specified amount of CO_2 in the pure methane-air-flame data in regions where the free stream oxygen was not affected. In calculations made with this new initial data, the agent entered the flame zone quickly through diffusion (in ~ 300 time steps) all along the flame simultaneously.

Calculations made with different concentrations of added CO_2 suggest that when the CO_2 volume fraction was $< 10\%$ (i.e., oxygen $> 18.9\%$ and nitrogen $> 71.1\%$), no significant change to the flame shape was observed. Results obtained for 10% of CO_2 volume fraction are shown in Fig. 4(a) with the distributions of temperature and CO_2 plotted on the left and right sides, respectively. The flame is anchored to the burner tip and is oscillating due to the vortices formed on the airside. However, the flame temperature decreased slowly with the added- CO_2 concentration. It has been reduced to 1750 K from 1880 K for 10% CO_2 added in the air stream. Because of this drop in temperature and increase in density of the air+ CO_2 surrounding the flame, the oscillation frequency is also changed slightly. For concentrations between 10 and 14.5% , the flame was separated (< 4 mm) from the burner lip and stabilized at a new location. An instantaneous solution of the computed flame for 14.5% CO_2 is shown in Fig. 4(b). As is evident from this plot that the flame base has been moved inside and downstream of the burner lip by ~ 4 mm. Interestingly, the flame oscillation in the base region has increased significantly. As a result, the base of the flame moved back and forth between the burner lip and the location shown in Fig 4(b) with time. The separation between the burner lip and the flame base allowed more air and CO_2 to enter the flame and provided partially premixed flow conditions. When the concentration of the added CO_2 was increased to a value $> 14.5\%$, the flame was completely blown out of the computational domain. An instantaneous solution of the blowout process is shown in Fig. 4(c) for the 15% added- CO_2 case. Because of the very low fuel flow rate, the flame has collapsed to the center and traveled downstream as it could not be stabilized at any location in the flow field. The large vortex (which developed at the base while the flame was swept by the added CO_2) is still present at the burner tip. Further calculations of this flame show it to be completely blown out of the computational domain. The experimental result for the extinction volume fraction of CO_2 in the air stream is 0.161 ± 0.005 for an oxidizer stream velocity of 10.7 cm/s.

Hence, the calculated extinction volume fraction of 14.5 % agrees reasonably well with that measured in the experiment. This close agreement is very encouraging for these first calculations of the extinction of cup-burner flames by fire suppression agents, since the calculations include both chemical effects and fluid-dynamic instabilities.

The computed evolution of temperature at 30 mm above the burner for 10 %, 14.4 % and 15 % added- CO_2 cases are shown in Figs. 5(a), 5(b), 5(c), respectively. From these figures it is evident that the amplitude of the flame oscillations is increasing with the added CO_2 . And also, the fluctuations deviate significantly from perfectly periodic ones for concentrations $> 10\%$; which, in part, is due to the back and forth flame propagation taking place between the flame base and the burner tip in the detached-flame-base cases. Fig. 5(c) shows how the flame base is collapsing at the axis as it travels downstream in the 15 % CO_2 case.

The variations of flame temperature and peak heat release rate along the flame zone are shown in Fig. 6(a) for 0 %, 10 % and 14.5 % CO_2 flames. The flame temperature dropped to 1620 K and the peak heat-release rate near the flame base decreased from 320 to 170 $\text{J}/\text{cm}^3/\text{s}$ with the critical concentration of CO_2 . Interestingly, the heat release rate in the downstream locations has initially increased with the addition of CO_2 up to 10 % and then decreased for further addition.

Radial distributions of temperature and fuel and oxygen concentrations for the three flames in Fig. 6(a) at 10 mm above the burner are plotted in Fig. 6(b). Several interesting behaviors of these flames may be noted from this figure. 1) The slope of the temperature profile on the airside is the same in all the flames. 2) Consumption of fuel is decreasing and the fuel jet column is getting longer with the addition of CO_2 . 3) Flame diameter is decreasing with CO_2 concentration.

Calculations made with different CO_2 concentrations indicate that the cup-burner flame extinguishes through the blowout process—meaning that, the flame at the base detaches from the burner first, similar to lifting of jet diffusion flames [27], and then shifts downstream till it clears off from the computational domain. This blowout behavior was the same even for the case with CO_2 concentration of 20 %. Thus, using the cup burner configuration, it may be difficult to obtain global extinction of the flame. As the concentration of CO_2 is increased, however, the time for the flame base to blowout of the computational domain does decrease. Nonetheless, the absolute concentration of CO_2 required to quench the flame entirely is important to know as that value represents the concentration of CO_2 required to extinguish a most stable flame such as pool fire.

Opposed-jet diffusion flames offer flame structures without having an edge or base. On the other hand, these flames are subjected to different strain rates depending on the inflow conditions. In order to obtain the absolute concentration of CO_2 needed for extinguishing a flame, calculations were also made for opposed-jet diffusion flame for two different strain-rate conditions. A low strain rate (global) of 30 s^{-1} was achieved by forcing a 0.2-m/s fuel jet toward a 0.2-m/s air jet that is separated by 13 mm from the former. Similarly, a moderate global strain rate of 90 s^{-1} was obtained between 0.6-m/s fuel and air jets. Complete axisymmetric 2D simulations (not just 1D along the stagnation line) were made using the CFD code described earlier. Results in the form of temperature and CO_2 distributions are plotted in Figs. 7(a) and 7(b) for the low-strain-rate flame and those for the moderate-strain-rate case are plotted in Figs. 7(c) and 7(d). Among these results, Figs. 7(a) and 7(c) represent the flames with 0 % added CO_2 and Figs. 7(b) and

7(d) represent those with maximum amounts of CO₂ that can be added without extinguishing the flame. For the low- and moderate-strain-rate cases these maximum CO₂ concentrations were found to be 16.4 % and 10.4 %, respectively. These limits were obtained by computing intermediate steady state flames by increasing the CO₂ concentration in the air stream in steps. The variations of flame temperature and peak CO₂ produced in the flame zone as functions of added CO₂ are shown in Fig. 8. The temperature of the low-strain flame with 0 % CO₂ added is slightly above that of the cup burner while that of the moderate-strain flame is slightly below. Consistent with these temperatures, the limiting volume fraction of CO₂ for the cup burner (14.5 % computed and 16.1 % measured) falls between the two cases, but nearer to the low-strain opposed-jet flame extinction volume fraction (16.4 %). Interestingly, both flames extinguished at ~1580 K. The constant temperature indicates that the extinction limits of opposed-jet diffusion flames are controlled primarily by kinetics as was observed experimentally [28]. As described before, the cup-burner flame did not extinguish simultaneously at every location because the destabilization of the edge diffusion flame occurred before the global extinction. Incidentally, the cup-burner flame temperature at suppression was comparable yet somewhat higher (~1620 K) than that of the opposed-jet diffusion flames.

Distributions of heat release rate and species concentrations along the stagnation line are plotted in Fig. 9 for the low-strain opposed-jet flame for different concentrations of added CO₂. The heat release rate (~140 J/cm³s) in the opposed-jet flame at the critical concentration of CO₂ was somewhat lower than that (~170 J/cm³s) in the cup-burner flame. This also suggests that the cup-burner flame in Fig. 4(c) is not extinguished through the global extinction of combustion reactions and, as discussed earlier, is extinguished rather due to the premature destabilization of the flame base.

CONCLUSIONS

A periodically oscillating, pure-methane-air diffusion flame formed over a cup burner was used to explore the suppression characteristics of CO₂. This laminar flame, calculated for a small fuel flow rate and a low-speed annular air flow, generated large-scale, low-frequency (~ 10 Hz), organized buoyancy-induced vortices on the air side of the flame that are similar to those observed in pool fires. A detailed chemical-kinetics model GRI-V1.2 having 31 species and 346 elementary-reaction steps was incorporated into an axisymmetric CFD model for the investigation of the effects of CO₂ on methane combustion. Simulations were performed on a Pentium III 1-GHz-based Personal Computer and the typical execution time was ~24 h per case.

To explore the suppression mechanism resulting from CO₂, it was added only to the airflow in this study. It was observed that the size of the outer vortices and the flicker frequency increase with the addition CO₂. The addition of CO₂ reduced the flame temperature ~260 K down to ~1620 K before it was quenched. Between 10 % and 14.5 % CO₂ volume fraction, the diffusion flame base shifted slowly toward a downstream location and became stabilized within 5 mm from the jet exit and finally for concentrations > 14.5 %, the flame base moved downstream rapidly until it clears the computational domain. Flame structures obtained for CO₂ volume fractions of 10 %, 14.5 % and 15 % CO₂ are compared with those obtained for the pure methane-air jet diffusion flame. Calculations were also made for axisymmetric opposed-jet flames for different strain-rate cases. Low-strain (30 s⁻¹) opposed-jet flames extinguished for CO₂ volume fractions > 16.4 % while the moderate-strain (90 s⁻¹) flame extinguished for

volume fractions $> 10.4\%$, both at ~ 1580 K. The constant temperature suggests that the extinction limits are controlled primarily by kinetics. Therefore, the mechanisms responsible for the suppression of cup-burner and opposed-jet flames are quite different. The flame base of the cup-burner was destabilized with the addition of CO_2 and then moved downstream in search of a new stabilization location. For concentrations $> 14.5\%$ flame based moved out of the computational domain, as it could not find a stabilization point within the domain. The unsteady flickering motion of the flame accelerated the quenching process. On the other hand, the opposed-jet flame was extinguished through the global extinction of flame chemistry.

ACKNOWLEDGMENTS

This work was supported by the Office of Biological and Physical Research, NASA, Washington, D. C. The first author would like to thank Dr. Mel Roquemore of Wright Laboratory for the stimulating discussions on buoyant flames.

REFERENCES

1. Anderson, S. O., *Fire J.*, Vol. 81, 1987, p. 56 and 118.
2. Gann, R. G. (Ed), *Halogenated Fire Suppressants*, ACS Symposium Series No. 16, The American Chemical Society, 1975.
3. Biordi, J. C., Lazzara, C. P., and Papp, J. F., *Fourteenth Symposium (International) on Combustion*, The Combustion Institute, Pittsburgh, 1973, p. 367.
4. Westbrook, C. K., *Combust. Sci. Technol.* Vol. 34, 1983, p. 201.
5. Nyden, M. R., Linteris, G. T., Burgess, D. R. F., Jr., Westmoreland, P. R., Tsang, W., and Zachariah, M., in *Evaluation of Alternative In-Flight and Dry Bays* (Eds. W. L. Grosshandler, R. G. Gann, and W. M. Pitts), National Institute of Standards and Technology, Gaithersburg, MD, 1994, NIST SP 861, p. 467.
6. Linteris, G. T., and Truett, L., *Combust. Flame*, Vol. 105, 1996, p. 15.
7. Linteris, G. T., Burgess, D. R., Jr., Babushok, V., Zachariah, M., Tsang, W., and Westmoreland, P., *Combust. Flame*, Vol. 113, 1998, p. 164.
8. Milne, T. A., Green, C. L., and Benson, D. K., *Combust. Flame*, Vol. 15, 1970, p. 255.
9. Seshadri, K., and Ilincic, N., *Combust. Flame*, Vol. 101, 1995, p. 271.
10. Ellzey, J. L., Laskey, K. J., and Oran, E. S., (1989), in *Dynamics of Deflagrations and Reactive Systems: Flames*, A. L. Kuhl, J. C. Leyer, A. A. Borisov, and W. A. Sirignano, Eds., Vol. 131, *Progress in Astronautics and Aeronautics*, American Institute of Aeronautics and Astronautics, Washington, D. C., 1989, p. 179.
11. Yamashita, H., Kushida, G., and Takeno, T., *Proc Roy Soc of London A*, Vol. 431, No. 1882, 1990, p. 301.
12. Davis, R. W., Moore, E. F., Roquemore, W. M., Chen, L.-D., Vilimpoc, V., and Goss, L. P., *Combustion and Flame*, Vol. 83, Nos. 3/4, 1991, pp. 263-270.
13. Katta, V. R., Goss, L. P., and Roquemore, W. M., *AIAA Journal*, Vol. 32, No. 1, 1994, p. 84.
14. Patnaik, G. and Kailasanath, K., *Combustion and Flame*, Vol. 99, No. 10, 1994, p. 247.
15. Kaplan, C. R., Oran, E. S., Kailasanath, K., and Ross, H. D., *26th Symposium (International) on Combustion*, The combustion Institute, Pittsburgh, PA, 1996, p. 1301.
16. Takagi T., and Xu, Z., *Combustion and Flame*, Vol. 96, Nos. 1 and 2, 1994, p. 50.
17. Katta, V. R., and Roquemore, W. M., *Combustion and Flame*, Vol. 100, No. 1, 1995, p. 61.
18. Roquemore W. M., and Katta, V. R., *Journal of Visualization*, in press Jan. 2000.
19. Frenklach, M., Wang, H., Goldenberg, M., Smith, G. P., Golden, D. M., Bowman, C. T., Hanson, R. K., Gardiner, W. C., V. Lissianski, V., Technical Report No. GRI-95/0058, Gas Research Institute, Chicago, IL, November 1, 1995.
20. Annon., *Computational Submodels*, International Workshop on Measurement and Computation of Turbulent Nonpremixed Flames., <http://www.ca.sandia.gov/tdf/Workshop/Submodels.html>, 2001.
21. Katta, V. R., Goss, L. P., and Roquemore, W. M., *Int. J. Num. Methods Heat Fluid Flow*, Vol. 4, No. 5, 1994, p. 413.
22. National Fire Protection Agency, *Standard on Clean Agent Fire Extinguishing Systems*, NFPA 2001 (1994).
23. Hirst, B. and Booth, K., *Fire Technol.* 13:296 (1977).

24. Linteris, G.T. and Gmurczyk, G.W., in *Fire Suppression System Performance of Alternative Agents in Aircraft Engine and Dry Bay Laboratory Simulations* (R.G. Gann, Ed.), National Institute of Standards and Technology, Gaithersburg, MD, 1995.
25. Katta, V. R., and Roquemore W. M., *AIAA J*, Vol. 36, No. 11, 1998, p. 2044.
26. Roquemore, W. M., Chen, L-D., Goss, L. P., and Lynn, W. F., *Turbulent Reactive Flows*, edited by R. Borghi and S. N. B. Murthy, Vol. 40, *Lecture Notes in Engineering*, Springer-Verlag, Berlin, 1989, p. 49.
27. Takahashi, F., and Katta, V. R., *Proceedings of the Combustion Institute*, Vol. 28, 2000, pp. 2071-2078.
28. Ishizuka, S., and Tsuji, H., *Eighteenth Symposium (International) on Combustion*, The Combustion Institute, Pittsburgh, 1981, p. 695.

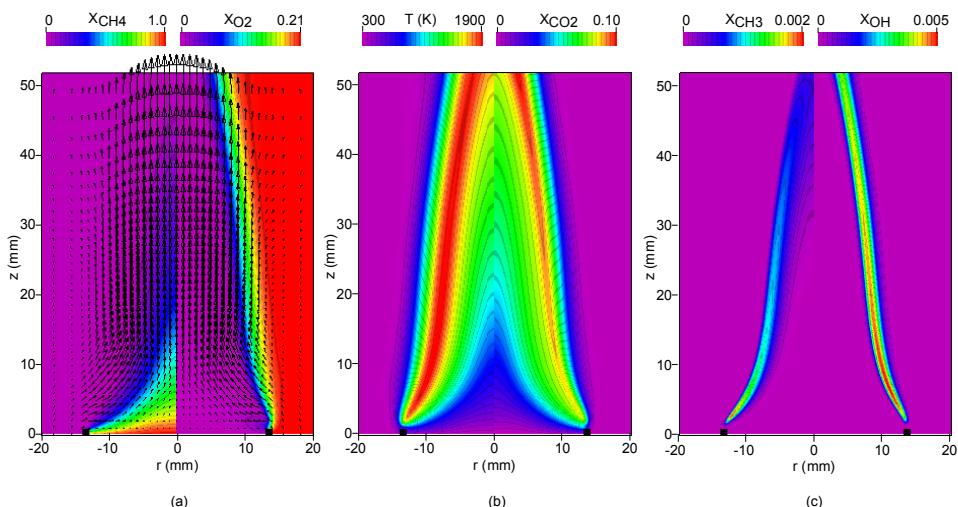


Fig. 1. Instantaneous flame simulated for a cup burner with 0.107 m/s annular airflow (no CO₂). (a) Velocity field superimposed over fuel-concentration distribution (left) and over oxygen-concentration distribution (right), (b) temperature field (left) and CO₂ distribution (right), (c) CH₃ (left) and OH (right) concentration fields.

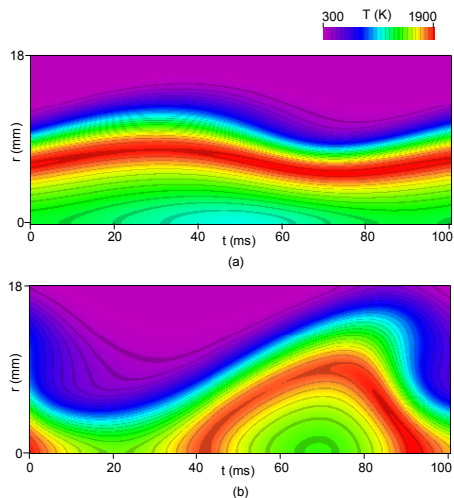


Fig. 2. Evolution of temperature at (a) 30 mm and (b) 80 mm above the burner for no CO₂ in the airflow.

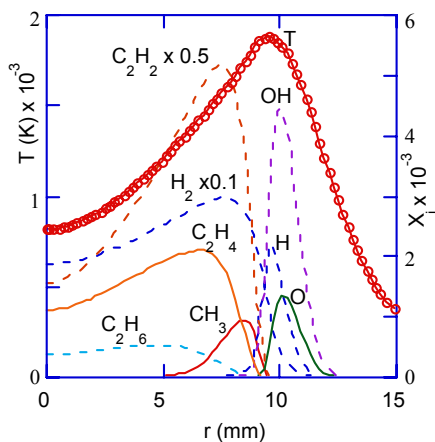


Fig. 3. Species and temperature distributions across the flame at 10 mm above the burner.

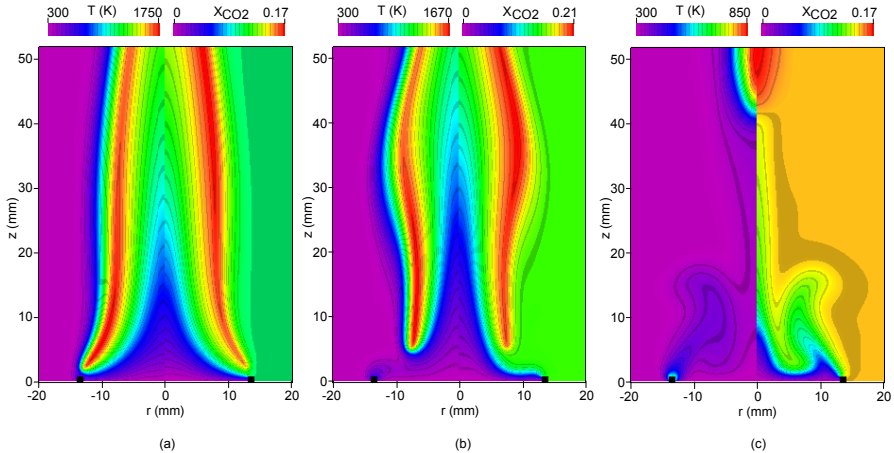


Fig. 4. Flames simulated for a cup burner for various concentrations of CO_2 added in airflow. Instantaneous temperature and CO_2 -concentration fields are shown on the left and right sides of each image, respectively. (a) For 10 % added CO_2 , (b) for limiting value of 14.5 % CO_2 , and (c) for slightly above the limit (15 %) CO_2 .

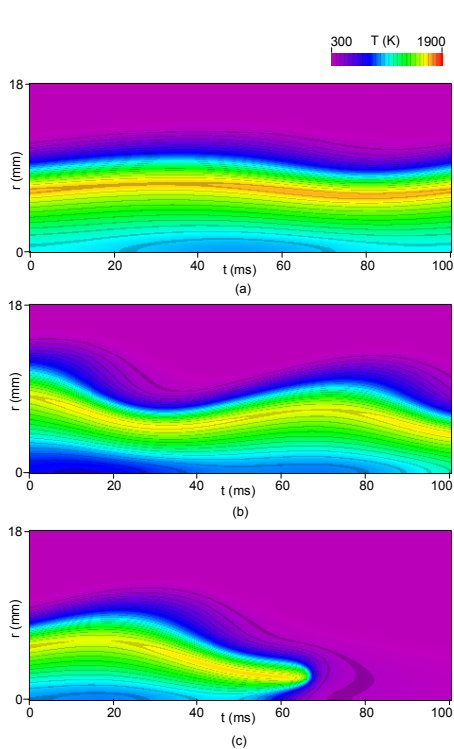


Fig. 5. Evolution of temperature at 30 mm above the burner for (a) 10 %, (b) 14.5 %, and (c) 15 % of CO_2 in airflow.

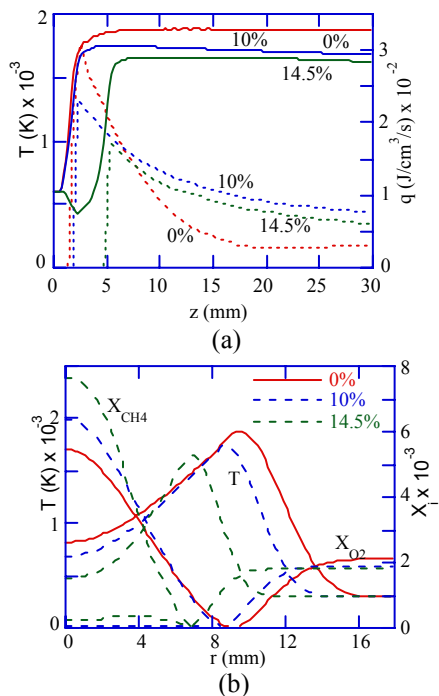


Fig. 6. Flame structures for different concentrations of CO_2 in airflow. (a) Temperature and heat-release rate along the flame surface. (b) Radial distributions of temperature and species at a location 10 mm above the burner.

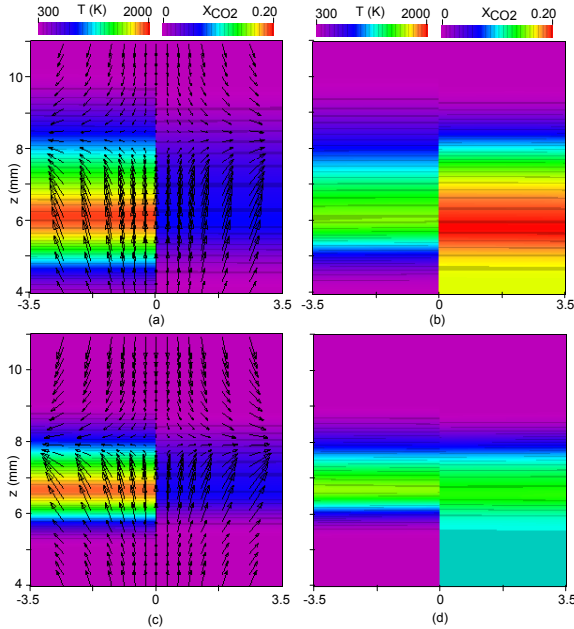


Fig. 7. Steady state, axisymmetric, opposed-jet flames simulated for different strain rate conditions. (a), (b) for 30 s^{-1} and (c), (d) for 90 s^{-1} global strain rates. (a), (c) with 0 % added CO_2 , and (b), (d) with critical concentrations of CO_2 added in airflow. Temperature and CO_2 -concentration fields are shown on the left and right sides of each image, respectively. In addition, velocity fields are superimposed in (a) and (c).

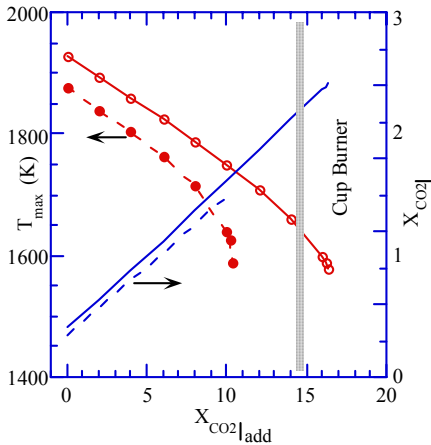


Fig. 8. Variation of flame temperature and peak CO_2 concentration with the amount of CO_2 added to the airflow. Solid lines represent the data for 30 s^{-1} strained flame and broken lines represent those for 90 s^{-1} strained flame.

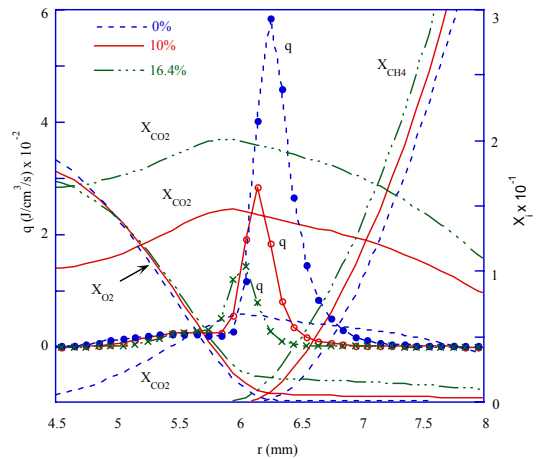


Fig. 9. Distributions of heat-release rate and species mole fractions along stagnation line for 30 s^{-1} strained opposed-jet flame for different concentrations of added CO_2 .